BUOYANCY-INDUCED CONVECTION OF WATER-BASED NANOFLUIDS IN DIFFERENTIALLY-HEATED HORIZONTAL SEMI-ANNULI

by

Alessandro QUINTINO, Elisa RICCI, Emanuele HABIB, and Massimo CORCIONE[*]

Department of Thechnical Physics (DIAEE), Sapienza University of Rome,
Rome, Italy

A two-phase model based on the double-diffusive approach is used to perform a numerical study on natural convection of water-based nanofluids in differentially-heated horizontal semi-annuli, assuming that Brownian diffusion and thermophoresis are the only slip mechanisms by which the solid phase can develop a significant relative velocity with respect to the liquid phase. The system of the governing equations of continuity, momentum, and energy for the nanofluid, and continuity for the nanoparticles, is solved by the way of a computational code which incorporates three empirical correlations for the evaluation of the effective thermal conductivity, the effective dynamic viscosity, and the thermophoretic diffusion coefficient, all based on a wide number of literature experimental data. The pressure-velocity coupling is handled through the SIMPLE-C algorithm. Numerical simulations are executed for three different nanofluids, using the diameter and the average volume fraction of the suspended nanoparticles, the cavity size, the average temperature, and the temperature difference imposed across the cavity, as independent variables. It is found that the impact of the nanoparticle dispersion into the base liquid increases remarkably with increasing the average temperature, whereas, by contrast, the other controlling parameters have moderate effects. Moreover, at temperatures of the order of room temperature or just higher, the heat transfer performance of the nanofluid is significantly affected by the choice of the solid phase material.

Key words: *nanofluid, natural convection, horizontal semi-annuli,
two-phase approach, enhanced heat transfer*

Introduction

Buoyancy-driven convection of nanofluids in horizontal cavities bounded by differentially-heated concentric circular walls has gained a lot of interest in the last decade, owing to its relevance to several potential thermal engineering applications, such as heat exchangers, solar collectors, and the cooling of electronic devices, just to mention a few.

The studies readily available in the literature on this topic were carried out numerically by Abu-Nada *et al.* [1], Abu-Nada [2, 3], Soleimani *et al.* [4], Yu *et al.* [5], Parvin *et al.* [6], Ashorynejad *et al.* [7], Sheikholeslami *et al.* [8], Corcione *et al.* [9], Sheikhzadeh *et al.* [10],

_____
[*] Corresponding author, e-mail: massimo.corcione@uniroma1.it

2644

Quintino, A., *et al.*: Buoyancy-Induced Convection of Water-Based Nanofluids in ...
THERMAL SCIENCE: Year 2017, Vol. 21, No. 6A, pp. 2643-2660

Table 1. Summary of the numerical studies performed on natural convection of nanofluids in horizontal cavities bounded by differentially-heated concentric circular walls

Year	Author(s)	Approach	Nanofluid	Particle size	Volume fraction	Rayleigh number	Diameter ratio	Geometry
2008	Abu-Nada et al. [1]	Single-phase	$Cu+H_2O$ $Ag+H_2O$ $Al_2O_3+H_2O$ TiO_2+H_2O		0%-10%	10^3-10^5	1.4-2.6	Annulus
2009	Abu-Nada [2]	Single-phase	$Al_2O_3+H_2O$	47 nm	0%-9%	10^3-10^5	1.4-2.6	Annulus
2010	Abu-Nada [3]	Single-phase	$CuO+H_2O$	29 nm	0%-9%	10^3-10^5	1.4-2.6	Annulus
2012	Soleimani et al. [4]	Single-phase	$Cu+H_2O$		0%-6%	10^3-10^5	2	Annular segment + Semi-annulus
2012	Yu et al. [5]	Single-phase	$CuO+H_2O$	30 nm	0%-4%	10^4 - 10^6	1.5-3	Annulus
2012	Parvin et al. [6]	Single-phase	$Al_2O_3+H_2O$		0%-15%	$1.47 \cdot 10^3$-$8.81 \cdot 10^6$	5	Annulus
2013	Ashorynejad et al. [7]	Single-phase	$Ag+H_2O$		0%-6%	10^3-$5 \cdot 10^4$	2-4	Annulus
2013	Sheikholeslami et al. [8]	Single-phase	$Cu+H_2O$		0%-6%	10^3-10^5	2	Semi-annulus
2013	Corcione et al. [9]	Two-phase	$Al_2O_3+H_2O$	25-100 nm	0%-6%	10^1-10^7	2-5	Annulus
2013	Sheikhzadeh et al. [10]	Single-phase	$Cu+H_2O$		0%-10%	10^3-10^5	2.6	Annulus
2014	Sheikholeslami and Ganji [11]	Single-phase	Fe_3O_4+H2O		0%-4%	10^3-10^5	1.7	Semi-annulus
2014	Sheikholeslami et al. [12]	Two-phase				10^5	2	Annular segment
2015	Arbaban and Salimpour [13]	Single-phase	$Cu+H_2O$ $Al_2O_3+H_2O$ TiO_2+H_2O		0%-10%	10^3-10^5	1.8-2.6	Annulus
2015	Fallah et al. [14]	Single-phase	$Al_2O_3+H_2O$	47 nm	0%-4%	10^3-10^5	1.4-5	Annulus
2015	Bezi et al. [15]	Single-phase	$Au+H_2O$ $Cu+H_2O$ $Al_2O_3+H_2O$ $CuO+H_2O$		0%-8%	10^3-10^5	2	Semi-annulus
2015	Seyyedi et al. [16]	Single-phase	$Cu+H_2O$		0%-6%	10^3-10^5	2-4	Annulus
2016	Oglakkaya and Bozkaya [17]	Single-phase	$Cu+H_2O$		0%-20%	10^3-10^5	2	Semi-annulus
2016	Zhang et al. [18]	Two-phase				10^3-10^6	2.5-10	Annulus
2016	Sheikholeslami and Chamkha [19]	Single-phase	Fe_3O_4+EG	< 50 nm	0%-5%	$5 \cdot 10^1$-$5 \cdot 10^2$	2	Annular segment

Quintino, A., *et al.*: Buoyancy-Induced Convection of Water-Based Nanofluids in ...
THERMAL SCIENCE: Year 2017, Vol. 21, No. 6A, pp. 2643-2660

2645

Sheikholeslami and Ganji [11], Sheikholeslami *et al.* [12], Arbaban and Salimpour [13], Fallah *et al.* [14], Bezi *et al.* [15], Seyyedi *et al.* [16], Oglakkaya and Bozkaya [17], Zhang *et al.* [18], and Sheikholeslami and Chamkha [19]. A survey of these papers is presented in tab. 1, in which indications on the modelling approach, the employed nanofluid, the geometry of the cavity, as well as the investigated ranges/values of the size and volume fraction of the suspended nanoparticles, the Rayleigh number based on the gap-width between the two cylindrical walls, and the ratio between the outer and inner diameters, are enumerated.

The typical conclusion of many of these studies is that the nanofluid heat transfer performance enhances as the amount of the dispersed solid phase is increased, although some considerations are worth being mentioned regarding the reliability of the results obtained. In fact, it is apparent that the majority of the listed works are based on the single-phase modelling, in which nanofluids are treated as pure fluids assuming that the solid and liquid phases are in local thermal and hydrodynamic equilibrium, thus meaning that the effects of the slip motion occurring between the suspended nanoparticles and the base liquid on the heat transfer performance are completely neglected. In addition, in most studies the effective thermal conductivity and dynamic viscosity are calculated by the Maxwell-Garnett model [20] and the Brinkman equation [21], respectively, that, as well-known, more or less severely underestimates the heat transfer aptitude and the rheological behaviour of nanofluids. On the other hand, in the few studies based on the two-phase approach, either the thermophoretic velocity of the nanoparticles is underestimated [9], owing to the use of the MacNab-Meisen relationship [22] (whose applicability to nanofluids neither has ever been demonstrated nor ensures to reproduce the existing experimental data of buoyancy-induced enclosed flows of nanofluids), or, once the governing equations are expressed in dimensionless form [12, 18], the simulations are executed by imposing assigned solid-phase concentrations at the heated and cooled walls (which seems unrealistic since such concentrations cannot be known a priori), and using values of the Lewis number extremely low compared with the order of magnitude usual for nanofluids.

Framed in this general background, a comprehensive numerical study on buoyancy-driven convection of water-based nanofluids in differentially-heated horizontal semi-annuli is executed using a two-phase model based on the double-diffusive approach, in the hypothesis that Brownian diffusion and thermophoresis are the only slip mechanisms by which the solid phase can develop a significant relative velocity with respect to the liquid phase. The model developed incorporates three empirical correlations for the calculation of the effective thermal conductivity, the effective dynamic viscosity, and the thermophoretic diffusion coefficient, all based on a high number of experimental data available in the literature from diverse sources, and validated using relations from other authors and experimental data different from those employed in generating them. Primary scope of the paper is to investigate in what measure the nature, size and average volume fraction of the suspended nanoparticles, as well as the diameters of the inner and outer cylindrical walls, the average temperature, and the temperature difference imposed across the cavity, affect the basic heat and fluid flow features, as well as the thermal performance of the nanofluid.

Mathematical formulation

The horizontal semi-annular space existing between a pair of coaxial long half cylinders facing upwards is filled with a nanofluid. The inner half cylinder, having a radius, R_i, is heated at a uniform temperature, T_h, while the outer half cylinder, having a radius, R_o, is cooled at a uniform temperature, T_c. The remaining two boundaries are assumed to be adiabatic, as sketched in fig. 1, in which the reference polar co-ordinate system (r, θ) is also represented, where r is

2646

Quintino, A., *et al.*: Buoyancy-Induced Convection of Water-Based Nanofluids in ...
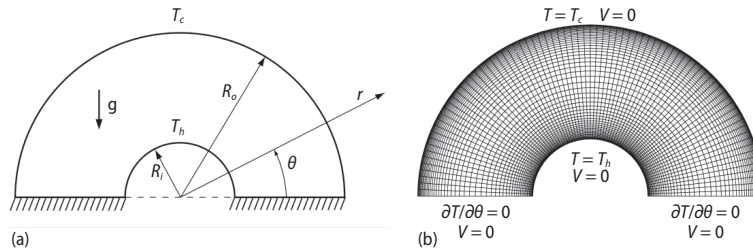THERMAL SCIENCE: Year 2017, Vol. 21, No. 6A, pp. 2643-2660

Figure 1. Sketch of the geometry and co-ordinate system (a) and of the discretization grid and boundary conditions (b)

measured from the centre of both cylinders, and θ is measured anti-clockwise. A zero-surface emissivity is assumed for all the confining walls, which physically corresponds to perfectly polished surfaces, thus implying that the present situation involves pure natural convection, *i. e.*, absence of surface-to-surface radiative heat transfer. The resulting buoyancy-induced flow is considered to be 2-D, laminar and incompressible, with negligible viscous dissipation and pressure work. It is assumed that the suspended nanoparticles and the base liquid are in local thermal equilibrium, and that Brownian diffusion and thermophoresis are the only slip mechanisms by which, in the absence of turbulent effects, the nanoparticles can develop a significant relative velocity with respect to the base liquid, as discussed by Buongiorno [23]. Another assumption made in the derivation of the model is that the effective properties of the nanofluid vary with temperature, other than being locally dependent on the concentration of the suspended solid phase. Finally, the Dufour effect, *i. e.*, the heat transfer associated with the nanoparticle motion relative to the base fluid, is neglected, being at least five orders of magnitude lower compared with heat conduction and convection, which was the same conclusion reached by Buongiorno [23].

In these hypotheses, the governing equations of continuity, momentum, and energy for the nanofluid, and the equation of continuity for the nanoparticles, reduce to:

$$\frac{\partial \rho_n}{\partial t} + \nabla(\rho_n \vec{V}) = 0 \tag{1}$$

$$\frac{\partial(\rho_n \vec{V})}{\partial t} + \nabla(\rho_n \vec{V}\vec{V}) = \nabla\boldsymbol{\tau} + \rho_n \vec{g} \tag{2}$$

$$\frac{\partial(\rho_n c_n T)}{\partial t} + \nabla(\rho_n \vec{V} c_n T) = \nabla(k_n \nabla T) \tag{3}$$

$$\frac{\partial(\rho_n m)}{\partial t} + \nabla(\rho_n \vec{V} m) = -\nabla\vec{J}_p \tag{4}$$

where t is the time, $\vec{V}$ – the velocity vector having radial and tangential components U and V, $\boldsymbol{\tau}$ – the stress tensor, $\vec{g}$ – the gravity vector, $\vec{J}_p$ – the nanoparticle diffusion mass flux, T – the temperature, m – the mass fraction (also called concentration) of the suspended nanoparticles, ρ_n – the effective mass density, c_n – the effective specific heat at constant pressure, and k_n – the effective thermal conductivity. Assuming that the nanofluid has a Newtonian behaviour − as, *e. g.*, demonstrated by Das *et al.* [24], Prasher *et al.* [25], He *et al.* [26], Chen *et al.* [27], Chevalier *et al.* [28], and Cabaleiro *et al.* [29] − the stress tensor can be expressed:

$$\boldsymbol{\tau} = -\left(p + \frac{2}{3}\mu_n \nabla\vec{V}\right)\mathbf{I} + \mu_n\left[\nabla\vec{V} + \left(\nabla\vec{V}\right)^t\right] \tag{5}$$

where p is the pressure, μ_n – the effective dynamic viscosity, and $\mathbf{I}$ – the unit tensor. Superscript t indicates the transpose of $\nabla \vec{V}$. The nanoparticle diffusion mass flux is calculated as the sum of the Brownian and thermophoretic diffusion terms in the hypothesis of dilute mixture (*i. e.*, low mass fraction), thus obtaining:

$$\vec{J}_p = -\rho_n \left(D_B \nabla m + D_T \frac{\nabla T}{T} \right) \tag{6}$$

where D_B and D_T are the Brownian and thermophoretic diffusion coefficients, respectively.

At this stage, it seems worth pointing out that the relation existing between the nanoparticle mass fraction, m, and the most widely used nanoparticle volume fraction, φ, is:

$$\rho_s \varphi = \rho_n m \tag{7}$$

where ρ_s is the mass density of the solid nanoparticles.

The Brownian diffusion coefficient, D_B, is given by the Stokes-Einstein equation [30]:

$$D_B = \frac{k_b T}{3\pi \mu_f d_p} \tag{8}$$

in which $k_b = 1.38066 \cdot 10^{-23}$ J/K is the Boltzmann constant, μ_f – the dynamic viscosity of the base fluid, and d_p – the diameter of the suspended nanoparticles.

The thermophoretic diffusion coefficient, D_T, is expressed:

$$D_T = S_T \frac{\mu_f}{\rho_f} m \tag{9}$$

where ρ_f is the mass density of the base liquid, and S_T is the so-called thermophoresis parameter, that, for water-based nanofluids containing metal oxide nanoparticles, can be evaluated by the following correlation recently developed by Corcione *et al.* [31] on the basis of experimental data-sets reported in the literature by different research teams:

$$S_T = \left[1.5 \cdot 10^4 \left(\frac{k_s}{k_f} \right)^{-3} + 0.9 \right] \left[-16(\varphi_{av})^{2.35} + 0.0195 \right] \tag{10}$$

in which k_s and k_f are the thermal conductivities of the solid nanoparticles and the base fluid, respectively, and φ_{av} is the average volume fraction of the suspended nanoparticles.

The effective thermal conductivity, k_n, and the effective dynamic viscosity, μ_n, can be predicted using the following correlations produced by Corcione [32] using a wide number of experimental data obtained by several research groups:

$$\frac{k_n}{k_f} = 1 + 4.4 \, \mathrm{Re}_p^{0.4} \, \mathrm{Pr}_f^{0.66} \left(\frac{T}{T_{fr}} \right)^{10} \left(\frac{k_s}{k_f} \right)^{0.03} \varphi^{0.66} \tag{11}$$

$$\frac{\mu_n}{\mu_f} = \frac{1}{1 - 34.87 \left(\dfrac{d_p}{d_f} \right)^{-0.3} \varphi^{1.03}} \tag{12}$$

where Re_p is the nanoparticle Reynolds number, Pr_f – the Prandtl number of the base fluid, T_{fr} – the freezing point of the base liquid, and d_f – the equivalent diameter of a base fluid molecule.

The nanoparticle Reynolds number is defined:

$$\mathrm{Re}_p = \frac{\rho_f u_p d_p}{\mu_f} \tag{13}$$

in which u_p is the nanoparticle Brownian velocity calculated as the ratio between d_p and the time t_D required to cover such a distance, that, according to Keblinski *et al.* [33], is:

$$t_D = \frac{d_p^2}{6D_B} \tag{14}$$

where D_B is the Brownian diffusion coefficient defined in eq. (8). Hence:

$$\mathrm{Re}_p = \frac{2\rho_f k_b T}{\pi \mu_f^2 d_p} \tag{15}$$

The equivalent diameter of a base fluid molecule is calculated at the reference temperature $T_0 = 293$ K on the basis of the relation $M = \rho_{f0} V_m N$, where M, ρ_{f0}, and V_m are the molar mass, the mass density at temperature T_0, and the molecular volume of the base fluid, while $N = 6.022 \cdot 10^{23}$ mol^{-1} is the Avogadro number. If we express V_m as $(4/3)\pi(d_f/2)^3$, we obtain:

$$d_f = 0.1 \left[\frac{6M}{N\pi\rho_{f0}} \right]^{1/3} \tag{16}$$

Besides the fact that both eqs. (11) and (12) accurately interpolates the experimental data which they are based on, their strength has recently been tested by way of a comparative analysis with several experimental data-sets different from those used in generating them, which resulted in a rather good degree of agreement − see, *e. g.*, Corcione *et al.* [31, 34]. Additional validations can be found in the studies carried out by Ghanbarpour *et al.* [35] and by Akilu *et al.* [36].

The effective mass density, ρ_n, and the effective specific heat at constant pressure, c_n, are calculated by the customary mixing theory:

$$\rho_n = (1-\varphi)\rho_f + \varphi\rho_s \tag{17}$$

$$c_n = \frac{(1-\varphi)(\rho c)_f + \varphi(\rho c)_s}{(1-\varphi)\rho_f + \varphi\rho_s} \tag{18}$$

in which $(\rho c)_f$ and $(\rho c)_s$ are the heat capacities at constant pressure per unit volume of the base fluid and the solid nanoparticles. The validity of eqs. (17) and (18) was confirmed experimentally by Pak and Cho [37], and by Zhou and Ni [38], respectively.

The assigned boundary conditions are: (a) $T = T_h$, $\vec{V} = 0$, and $\vec{J}_p = 0$ at the heated inner half cylinder surface, (b) $T = T_c$, $\vec{V} = 0$, and $\vec{J}_p = 0$ at the cooled outer half cylinder surface, and (c) $\partial T/\partial \theta = 0$, $\vec{V} = 0$, and $\vec{J}_p = 0$ at the adiabatic surfaces. The initial conditions assumed throughout the whole enclosure are: (a) nanofluid at rest, *i. e.*, $\vec{V} = 0$, (b) uniform average temperature of the nanofluid, $T_{av} = (T_h + T_c)/2$, and (c) assigned uniform average mass fraction of the suspended nanoparticles, m_{av}.

Quintino, A., *et al.*: Buoyancy-Induced Convection of Water-Based Nanofluids in ...
THERMAL SCIENCE: Year 2017, Vol. 21, No. 6A, pp. 2643-2660

2649

Computational procedure

The system of the governing equations defined by eqs. (1)-(4), in conjunction with the boundary and initial conditions stated earlier, is solved through a control-volume formulation of the finite-difference method. The pressure-velocity coupling is handled using the SIMPLE-C algorithm introduced by Van Doormaal and Raithby [39], which is essentially a more implicit variant of the SIMPLE algorithm developed by Patankar and Spalding [40], extensively described in Patankar [41], whose employment usually results in convergence speed-up when strongly coupled problems have to be solved. Convective terms are approximated through the QUICK discretization scheme proposed by Leonard [42], whereas a second-order backward scheme is applied for time integration. The computational spatial domain is filled with a non-uniform structured grid, having a higher concentration of grid lines near the boundary walls as well as in the stagnation region at the top of the inner half cylinder, and a lower uniform spacing throughout the remainder interior of the cavity. Time discretization is chosen uniform. Starting from the assigned initial fields of the dependent variables, at each time-step the system of the discretized algebraic governing equations is solved iteratively by the way of a line-by-line application of the Thomas algorithm. A standard under-relaxation technique is enforced in all steps of the computational procedure so as to ensure an adequate convergence. Within each time-step, the spatial numerical solution of the velocity, temperature, and concentration fields is considered to be converged when the maximum absolute value of the mass source, as well as the relative changes of the dependent variables at any grid-node between two consecutive iterations, are smaller than the pre-specified values of 10^{-6} and 10^{-7}, respectively. Time-integration is stopped once steady-state is reached. This means that the simulation procedure ends when the relative difference between the incoming and outgoing heat transfer rates at the heated and cooled half cylinder surfaces, and the relative changes of the time-derivatives of the dependent variables at any grid-node between two consecutive time-steps, are smaller than the pre-assigned values of 10^{-6} and 10^{-8}, respectively.

Once steady-state is reached, the heat fluxes at the heated and cooled half cylinder surfaces, q_h and q_c, are obtained using the following expressions:

$$q_h = -(k_n)_h \frac{\partial T}{\partial r}\bigg|_{r=R_i} \tag{19}$$

$$q_c = -(k_n)_c \frac{\partial T}{\partial r}\bigg|_{r=R_o} \tag{20}$$

where $(k_n)_h$ and $(k_n)_c$ are the values of the effective thermal conductivity at temperatures T_h and T_c, respectively. The temperature gradients in eqs. (19) and (20) are evaluated by a second-order temperature profile embracing the wall-node and the two-adjacent fluid-nodes. The heat transfer rates added to the nanofluid by the heated half cylinder and withdrawn from the nanofluid by the cooled half cylinder, Q_h and Q_c, are then calculated:

$$Q_h = \int_0^\pi -(k_n)_h \frac{\partial T}{\partial r}\bigg|_{r=R_i} R_i \mathrm{d}\theta \tag{21}$$

$$Q_c = \int_0^\pi -(k_n)_c \frac{\partial T}{\partial r}\bigg|_{r=R_o} R_o \mathrm{d}\theta \tag{22}$$

in which the integrals are computed numerically by means of the trapezoidal rule.

The corresponding average Nusselt numbers for the heated and cooled half cylinders, Nu_h and Nu_c, are:

$$Nu_h = \frac{h_h D_i}{(k_n)_h} = \frac{2Q_h}{\pi(k_n)_h(T_h - T_c)} \qquad (23)$$

$$Nu_c = \frac{h_c D_o}{(k_n)_c} = \frac{2Q_c}{\pi(k_n)_c(T_c - T_h)} \qquad (24)$$

where $D_i = 2R_i$ and $D_o = 2R_o$ are the diameters of the inner and outer half cylinders, and h_h and h_c are the average coefficients of convection at the heated and cooled half cylinder surfaces.

Of course, since at steady-state the incoming and outgoing heat transfer rates are the same, we can write:

$$Q_h = -Q_c = Q \qquad (25)$$

where Q is the rate of heat transferred across the cavity.

Accordingly, on account of eqs. (23)-(25), the following relationship between Nu_h and Nu_c holds:

$$Nu_h(k_n)_h = Nu_c(k_n)_c \qquad (26)$$

Numerical tests related to the dependence of the results on the mesh spacing and time stepping have been methodically performed for several combinations of the six controlling parameters, *i. e.*, m_{av}, d_p, T_c, T_h, R_i, and R_o. Of course, the average temperature, T_{av}, in conjunction with the temperature difference between the inner and outer half cylinders, ΔT, may be taken as independent variables instead of T_c and T_h. Also, the diameter of the inner half cylinder, D_i, and the ratio between the outer and inner diameters, $\delta = D_o/D_i$, may be used as independent variables in place of R_i and R_o. Moreover, the average nanoparticle volume fraction, φ_{av}, can be used as an independent variable instead of m_{av}, owing to the following relationship derived by combining eqs. (10) and (16):

$$\varphi_{av} = \left[\left(\frac{1}{m_{av}} - 1\right)\frac{\rho_s}{\rho_f} + 1\right]^{-1} \qquad (27)$$

in which the values of the mass densities ρ_s and ρ_f are calculated at temperature T_{av}.

The discretization grids and time-steps used for computations are chosen in such a way that further refinements do not produce noticeable modifications either in the heat transfer rates or in the flow and volume fraction fields. Specifically, the percentage changes of the heat transfer rates, Q_h and Q_c, those of the maximum radial velocity on the vertical midplane, U_{max}, and tangential velocity on the plane located at $\theta = \pi/4$, V_{max}, as well as those of the maximum and minimum nanoparticle volume fractions on the vertical midplane, φ_{max} and φ_{min}, must be smaller than the pre-established accuracy value of 1%. The typical number of nodal points ($r \times \theta$) and time-step used for simulations lie in the ranges between 150×60 and 210×120, and between $5 \cdot 10^{-3}$ second and 10^{-2} second, respectively. Selected results of the grid and time-step sensitivity analysis conducted for $Al_2O_3 + H_2O$ are presented in tabs. 2-4. As an example, one of the discretization grids used for computations, with the indication of the applied boundary conditions, is depicted in fig. 1.

Quintino, A., *et al.*: Buoyancy-Induced Convection of Water-Based Nanofluids in ...
THERMAL SCIENCE: Year 2017, Vol. 21, No. 6A, pp. 2643-2660

2651

Table 2. Grid sensitivity analysis for $Al_2O_3 + H_2O$, $\varphi_{av} = 0.02$, $T_{av} = 315$ K, $\Delta T = 10$ K, and $\Delta t = 5 \cdot 10^{-3}$ s

D_i [m]	δ	d_p	Mesh size	Q_{hot} [W]	φ_{max}	φ_{min}	$\|U_{max}\| \cdot 10^3$ [ms^{-1}]	$\|V_{max}\| \cdot 10^3$ [ms^{-1}]
0.03	2	25	80 × 20	234.04	0.1244	0.0566	5.53	4.06
			100 × 30	241.53	0.1209	0.0584	5.67	4.18
			150 × 60	246.05	0.1191	0.0596	5.75	4.24
			180 × 90	247.55	0.1187	0.0601	5.79	4.28
0.03	4	25	80 × 20	272.27	0.1284	0.0542	9.22	5.37
			100 × 30	277.66	0.1257	0.0552	9.50	5.50
			150 × 60	280.80	0.1240	0.0558	9.64	5.59
			180 × 90	281.70	0.1232	0.0559	9.71	5.63
0.07	4	25	150 × 60	498.99	0.1027	0.0565	11.93	8.70
			180 × 90	515.01	0.0985	0.0585	12.22	8.94
			210 × 120	522.63	0.0961	0.0596	12.37	9.11
			240 × 150	525.40	0.0952	0.0601	12.45	9.19
0.07	4	75	150 × 60	501.60	0.1089	0.0542	12.15	8.35
			180 × 90	511.60	0.1027	0.0572	12.51	8.69
			210 × 120	517.94	0.1003	0.0590	12.70	8.85
			240 × 150	519.60	0.0995	0.0595	12.76	8.92

Table 3. Grid sensitivity analysis for $Al_2O_3 + H_2O$, $D_i = 0.05$ m, $\delta = 3$, $d_p = 25$ nm, and $\Delta t = 5 \cdot 10^{-3}$ s

T_{av} [K]	ΔT [K]	φ_{av}	Mesh size	Q_{hot} [W]	φ_{max}	φ_{min}	$\|U_{max}\| \cdot 10^3$ [ms^{-1}]	$\|V_{max}\| \cdot 10^3$ [ms^{-1}]
300	5	0.01	80 × 20	130.35	0.0764	0.0296	5.62	3.45
			100 × 30	132.27	0.0749	0.0302	5.72	3.52
			150 × 60	133.63	0.0739	0.0307	5.79	3.57
			180 × 90	134.06	0.0734	0.0309	5.81	3.59
300	20	0.01	150 × 60	678.03	0.2589	0.0087	10.48	5.80
			180 × 90	693.70	0.2540	0.0090	10.77	5.93
			210 × 120	704.66	0.2506	0.0092	10.94	6.02
			240 × 150	711.14	0.2486	0.0093	11.03	6.06
330	20	0.01	100 × 30	1056.38	0.1155	0.0358	14.96	12.20
			150 × 60	1082.05	0.1129	0.0369	15.36	12.44
			180 × 90	1100.66	0.1112	0.0378	15.58	12.61
			210 × 120	1110.46	0.1103	0.0381	15.69	12.68
330	20	0.04	150 × 60	1139.53	0.2412	0.1198	14.87	11.25
			180 × 90	1169.73	0.2336	0.1235	15.25	11.48
			210 × 120	1191.13	0.2289	0.1264	15.46	11.65
			240 × 150	1202.21	0.2270	0.1272	15.59	11.73

Finally, with the scope to validate the numerical code used for the present study, four tests have been carried out. In the first test, the steady-state radial temperature profiles obtained for a differentially-heated horizontal annulus filled with water, assuming $m_{av} = 0$, have been compared with the temperature distributions detected experimentally by Kuehn and Goldstein [43] with the aid of a Mach-Zehnder interferometer for $T_{av} = 303.18$ K, $\Delta T = 0.371$ K, $R_i = 1.78$ cm, and $R_o = 4.625$ cm. In the second test, the steady-state results computed numerically, expressed in terms of the mean equivalent thermal conductivity k_{eq} (defined as the

2652

Quintino, A., *et al.*: Buoyancy-Induced Convection of Water-Based Nanofluids in ...
THERMAL SCIENCE: Year 2017, Vol. 21, No. 6A, pp. 2643-2660

**Table 4. Time-step sensitivity analysis for Al$_2$O$_3$ + H$_2$O, φ_{av} = 0.02,
D_i = 0.05 m, δ = 3, d_p = 25 nm, T_{av} = 330 K, and ΔT = 10 K**

Mesh size	Δt [s]	Q_{hot} [W]	φ_{max}	φ_{min}	$\|U_{max}\| \cdot 10^3$ [ms^{-1}]	$\|V_{max}\| \cdot 10^3$ [ms^{-1}]
	$5 \cdot 10^{-2}$	1264.57	0.2627	0.11709	16.42	13.11
280×120	10^{-2}	1216.55	0.2373	0.12330	15.67	11.95
	$5 \cdot 10^{-3}$	1191.13	0.2289	0.1264	15.46	11.65
	10^{-3}	1187.54	0.2269	0.12710	15.48	11.63

ratio between the actual heat transfer rate and the heat transfer rate that would occur by pure conduction in case of fluid at rest), have been compared with the experimental data obtained for water by Kuehn and Goldstein [43] using the same cited annular test-cell having R_i = 1.78 cm and R_o = 4.625 cm, for different values of T_{av} and ΔT. In the third test, the steady-state heat and mass transfer rates computed for the double-diffusive convection occurring around a horizontal isothermal circular cylinder suspended in a water-salt mixture having constant physical properties (Pr = 7, Le = 100), have been compared with a selection of numerical data published by Phanikumar and Mahajan [44]. In the fourth test, the strength of the whole computational code has been verified by numerically reproducing six sets of experiments performed using differentially-heated vertical enclosures filled with Al$_2$O$_3$ + H$_2$O by Putra *et al.* [45] for φ_{av} = 0.01 and 0.04, Chang *et al.* [46], for φ_{av} = 0.0131 and 0.0272, and Hu *et al.* [47] for φ_{av} = 0.0025 and 0.0077, in addition, the two sets of experiments executed by Wen and Ding [48] on a horizontal enclosure heated from below using TiO$_2$ + H$_2$O with φ_{av} = 0.00356 and 0.006, have also been reproduced. A good degree of agreement between our numerical results and the literature data was achieved in any validation test carried out, as for example displayed for the fourth test in fig. 2, in which the numerical solutions obtained for the ratio between the average Nusselt numbers of the nanofluid and the pure base fluid, Nu$_n$/Nu$_f$, plotted against the Rayleigh number of the nanofluid, Ra$_n$, are compared with the corresponding experimental data. Full details of the first three validation tests are available in the earlier study performed by Corcione *et al.* [9].
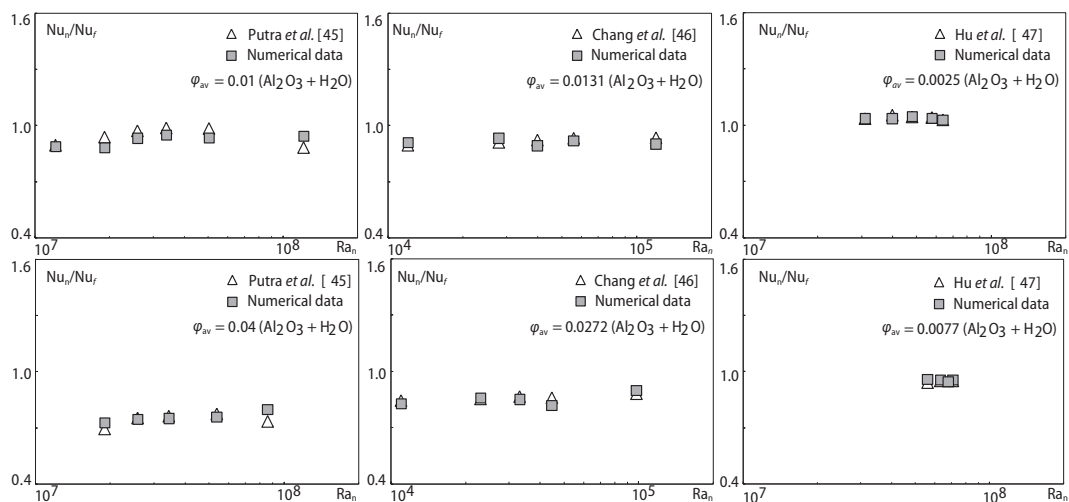
Figure 2. Comparison between the numerical values obtained for Nu$_n$/Nu$_f$ and the corresponding experimental data of Putra *et al.* [45], Chang *et al.* [46], and Hu *et al.* [47]

Quintino, A., *et al.*: Buoyancy-Induced Convection of Water-Based Nanofluids in ...
THERMAL SCIENCE: Year 2017, Vol. 21, No. 6A, pp. 2643-2660

2653

Results and discussion

Numerical simulations are performed using water-based nanofluids with suspended Al_2O_3, CuO or TiO_2 nanoparticles, for different values of (a) the average volume fraction of the solid phase, φ_{av}, in the range between 0 and 0.04, (b) the average diameter of the nanoparticles, d_p, in the range between 25 nm and 75 nm, (c) the average temperature, Tav, in the range between 300 K and 330 K, (d) the temperature difference imposed across the cavity, ΔT, in the range between 5 K and 20 K, (e) the diameter of the inner cylinder, D_i, in the range between 0.03 m and 0.07 m, and (f) the diameter ratio, δ, in the range between 2 and 4.

Typical local results are displayed in fig. 3, where ten streamlines, isotherm and isoconcentration contour lines equispaced between the detected minimum and maximum values of the stream function, temperature, and mass fraction, respectively, are plotted for $Al_2O_3 + H_2O$, $D_i = 0.05$ m, $\delta = 3$, $d_p = 25$ nm, $\varphi_{av} = 0.02$, $T_{av} = 315$ K, and $\Delta T = 10$ K. As expected, a flow
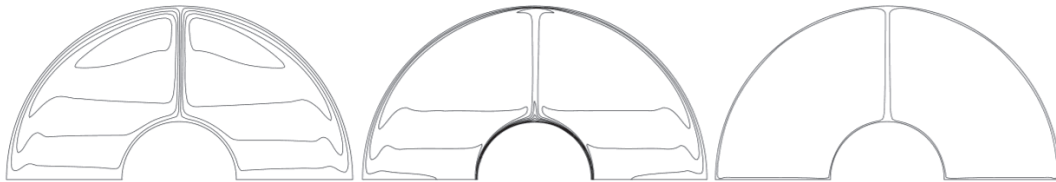
Figure 3. Streamline, isotherm and isoconcentration contours for $Al_2O_3 + H_2O$, $\varphi_{av} = 0.02$, $D_i = 0.05$ m, $\delta = 3$, $d_p = 25$ nm, $T_{av} = 315$ K, and $\Delta T = 10$ K

structure consisting of two counter-rotating kidney-shaped cells originates from the rising of the hot fluid above the heated half cylinder and the descent of two streams of cold fluid flowing down along the cooled half cylinder surface, symmetrically about the vertical midplane of the enclosure, as a result of the combined effects of the imposed temperature gradient and the concentration gradient consequent to the overall particle migration from hot to cold. The related temperature distribution is featured by a plume located in the middle of the cavity, two symmetric boundary-layers adjacent to the cooled half cylinder, and a pair of stratified fluid regions between the plume and each cooled side of the cavity. What seems now important to point out is the positive role played by the slip motion occurring between the solid and liquid phases in determining the heat transfer performance of the nanofluid. In fact, the nanofluid behaviour is primarily affected by the two opposite effects arising from the increase of both the thermal conductivity and the dynamic viscosity produced by the dispersion of the nanoparticles into the base liquid: the first effect, which tends to enhance the nanofluid heat transfer performance, prevails at small volume fractions of the suspended solid phase, whereas the second effect, which tends to degrade the nanofluid heat transfer performance, prevails at higher volume fractions. In addition, the effects of the two-phase behaviour give rise to the cited concentration gradient, which results in a cooperating solutal driving force. The situation is such that, as a rule, this extra buoyancy tends to compensate the increased friction consequent to the viscosity growth. Furthermore, the formation of a high-concentration thin nanofluid layer that stagnates above each bottom wall of the enclosure does not appreciably affect the circulation pattern. This means that the velocity and temperature fields of the nanofluid differ very little from those of the base liquid, as *e. g.* reported in fig. 4, where the distributions of V and T plotted along the plane located at $\theta = \pi/4$ are displayed for both $Al_2O_3 + H_2O$ and pure water. In particular, it can be observed that the temperature gradients at the inner and outer cylindrical walls are practically the same for the two profiles, thus implying that the beneficial effect of the increased thermal
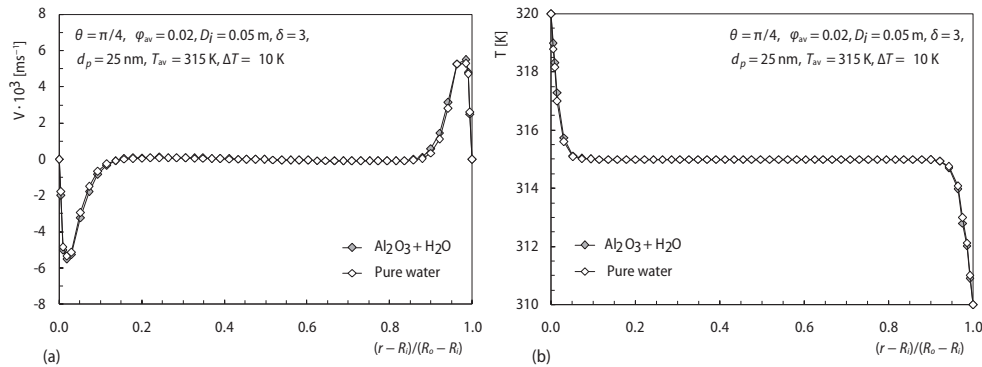
2654

Quintino, A., *et al.*: Buoyancy-Induced Convection of Water-Based Nanofluids in ...
THERMAL SCIENCE: Year 2017, Vol. 21, No. 6A, pp. 2643-2660

Figure 4. Distributions of V (a) and T (b) for Al$_2$O$_3$ + H$_2$O and pure water along the plane at $\theta = \pi/4$
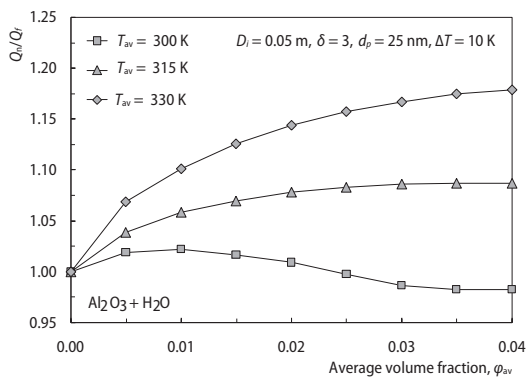
Figure 5. Distribution of Q_n/Q_f vs. φ_{av} for Al$_2$O$_3$ + H$_2$O, D_i = 0.05 m, δ = 3, d_p = 25 nm, and ΔT = 10 K, using T_{av} as a parameter

conductivity plays the major role in determining the heat transfer performance of the nanofluid. Hence, on account of eq. (11), a pronounced heat transfer enhancement has to be expected at high average temperatures, as shown in fig. 5, where a number of distributions of the ratio between the heat transfer rates across the nanofluid and the pure base fluid, Q_n/Q_f, are plotted *vs.* φ_{av} for different values of T_{av}. It can be noticed that the amount of heat exchanged by the nanofluid may be significantly higher than that exchanged by the pure base liquid, which is what happens at T_{av} = 330 K and φ_{av} = 0.04, that, for the exa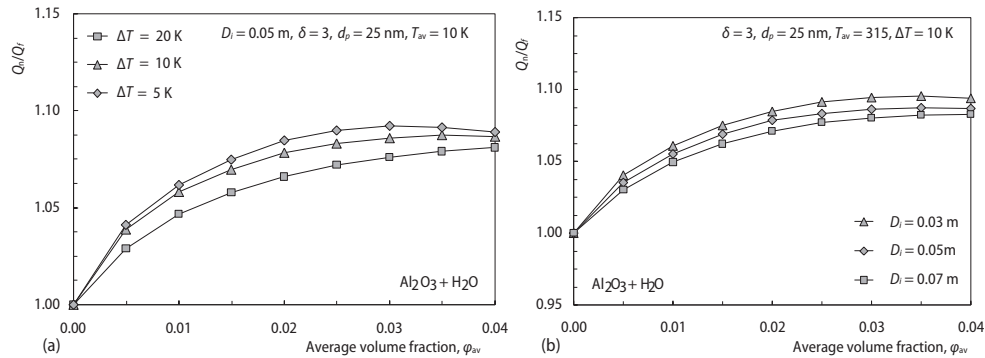mined configuration, corresponds to a 18% enhancement. On the other hand, at lower temperatures, *e. g.* T_{av} = 300 K, the limited increase of the thermal conductivity gives rise to a different situation. In fact, the dispersion of a progressively larger amount of nanoparticles into the base liquid results in a mild increase of the ratio Q_n/Q_f up to a point, due to the prevailing effect of the increased thermal conductivity. The value of φ_{av} corresponding to the peak of Q_n/Q_f can be identified as the optimal particle loading for maximum heat transfer, φ_{opt}. As φ_{av} is further increased above φ_{opt}, the ratio Q_n/Q_f decreases, which is a direct consequence of the prevailing effect of the dynamic viscosity growth. When the increased viscosity effect outweighs the increased thermal conductivity effect, the ratio Q_n/Q_f becomes lower than unity, thus meaning that the heat transfer rate in the nanofluid is lower than that in the pure base liquid, and the use of the nanofluid is detrimental.

The effects of the temperature difference imposed across the enclosure, the diameter of the inner cylinder, the diameter ratio, and the average diameter of the suspended nanoparticles, on the heat transfer performance of Al$_2$O$_3$ + H$_2$O are then pointed out in figs. 6 and 7, in which, for any independent variable, a number of distributions of the ratio Q_n/Q_f are plotted *vs.* φ_{av} using the variable itself as a parameter. Besides the fact that all these variables have moderate effects, it is apparent that Q_n/Q_f increases as ΔT and D_i are decreased and δ is increased. Conversely, as long as the temperature is low, Q_n/Q_f increases with decreasing d_p at

Figura 6. Distribution of Q_n/Q_f vs. φ_{av} for $Al_2O_3 + H_2O$, $D_i = 0.05$ m, $\delta = 3$, $d_p = 25$ nm, and $T_{av} = 315$ K, using ΔT (a) and D_i (b) as a parameter
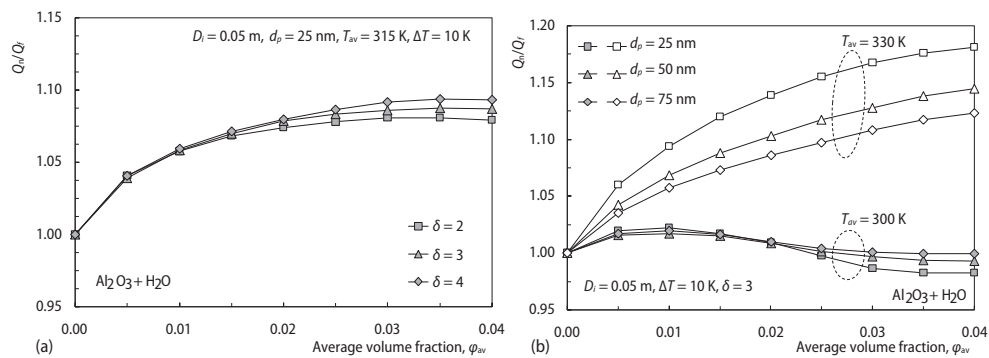
Figura 7. Distribution of Q_n/Q_f vs. φ_{av} for $Al_2O_3 + H_2O$, $D_i = 0.05$ m, $\delta = 3$, $d_p = 25$ nm, and $T_{av} = 315$ K, using δ (a) and d_p (b) as a parameter

small values of φ_{av}, whereas it decreases with decreasing d_p at higher values of φ_{av}. In fact, the thermal conductivity and the dynamic viscosity increase with decreasing the nanoparticle size, yet the effect of the increase in thermal conductivity prevails at low volume fractions, while the effect of the increase in dynamic viscosity prevails at high volume fractions. However, the value of φ_{av} at which such a behavior inversion occurs increases as T_{av} is increased, since k_n/k_f increases while μ_n/μ_f remains the same, which is the reason why at high temperature Q_n/Q_f decreases monotonically as d_p is increased.

Additionally, the effect of the solid phase material is shown in fig. 8. It can be seen that such an effect is crucial at low temperature, as reflected by the fact that Q_n/Q_f experiences a significant decrease if CuO nanoparticles are dispersed into water instead of Al_2O_3 nanoparticles, and an even more remarkable reduction if TiO_2 nanoparticles are used. This can be explained by considering that, based on eqs. (9) and (10), the thermophoretic diffusion coefficient increases when passing from.

The Al_2O_3 nanoparticles to CuO or TiO_2 nanoparticles, due to their lower thermal conductivity. As a consequence, the thickness of the stagnant nanofluid layers that form at the bottom walls of the cavity increases, which, despite the higher solutal buoyancy force, results in a limitation of the nanofluid circulation, and thus in a decrease of the heat transfer rate. Conversely, the effect of the solid phase material is weaker at high temperature. In fact, taking into account eqs. (6) and (8), the effects of the thermophoretic diffusion decrease as temperature is increased,
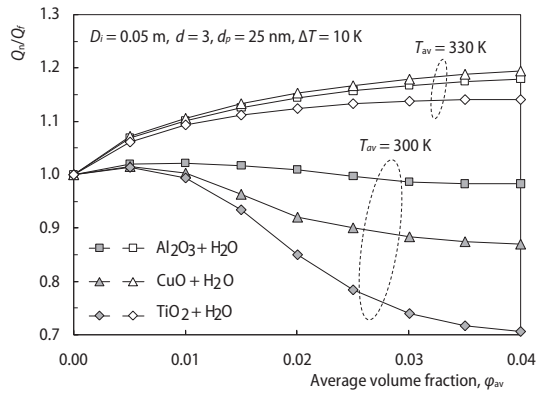
2656

Quintino, A., *et al.*: Buoyancy-Induced Convection of Water-Based Nanofluids in ...
THERMAL SCIENCE: Year 2017, Vol. 21, No. 6A, pp. 2643-2660

Figure 8. Distribution of Q_n/Q_f vs. φ_{av} for $D_i = 0.05$ m, $\delta = 3$, $d_p = 25$ nm, $\Delta T = 10$ K, and $T_{av} = 300$ K and 330 K, using the solid phase material as a parameter

while, at the same time, those of the Brownian diffusion increase, which implies that the overall nanoparticle mass flux from hot to cold decreases as the average temperature is increased. Accordingly, also the thickness of the stagnant nanofluid layers at the bottom of the enclosure decreases as temperature is increased, thus meaning that the flow structure for the three analysed nanofluids is similar. Indeed, for $Al_2O_3 + H_2O$ and $CuO + H_2O$ the shape of the circulation pattern is almost the same, which, combined with the higher solutal buoyancy force arising in $CuO + H_2O$ due to the higher mass density of CuO with respect to Al_2O_3, results in a slightly higher heat transfer performance of $CuO + H_2O$ compared to that of $Al_2O_3 + H_2O$.

The following pair of correlations is developed for predicting the average Nusselt numbers of pure water and $Al_2O_3 + H_2O$ at the cooled half cylinder surface, Nu_{fc} and Nu_c:

$$Nu_{fc} = 0.7 \frac{1}{\left(1 + \delta^{-3/5}\right)^{0.62}} \left[\frac{Pr_f}{0.42 + Pr_f} Ra_f\right]^{0.24} \quad \text{for} \quad \varphi_{av} = 0 \quad (28)$$

$$Nu_c = 0.263 \left[\frac{Pr_n}{0.08 + Pr_n} Ra_n\right]^{0.26} \left(\frac{\Delta T}{T_c}\right)^{-0.07} \delta^{0.2} \varphi_{av}^{0.0154} \quad \text{for} \quad 0 < \varphi_{av} \le 0.04 \quad (29)$$

for d_p in the range between 25 nm and 75 nm, T_{av} in the range between 300 K and 330 K, ΔT in the range between 5 K and 20 K, D_i in the range between 0.02 m and 0.08 m, and δ in the range between 2 and 4. The standard deviations of the error of eqs. (28) and (29) are 2% and 1.6%, respectively, whereas the percentage range of the relative error is ±3% for both of them, as shown in fig. 9. In the previous equations, Pr_f and Ra_f are the Prandtl and Rayleigh numbers of the base fluid, while Pr_n and Ra_n are the nanofluid effective Prandtl and Rayleigh numbers defined using the effective properties calculated at φ_{av}:
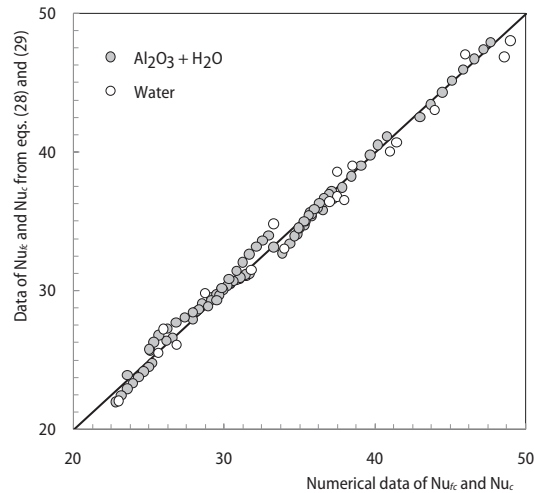
$$Pr_f = \frac{(c_f)_c (\mu_f)_c}{(k_f)_c}, \quad Ra_f = \frac{(\rho_f)_c (c_f)_c g\left[(\rho_f)_c - (\rho_f)_h\right] D_i^3}{(k_n)_c (\mu_n)_c} \quad (30)$$

$$Pr_n = \frac{(c_n)_c (\mu_n)_c}{(k_n)_c}, \quad Ra_n = \frac{(\rho_n)_c (c_n)_c g\left[(\rho_n)_c - (\rho_n)_h\right] D_i^3}{(k_n)_c (\mu_n)_c} \quad (31)$$

in which the properties with subscript c are calculated at temperature T_c, whereas the properties with subscript h are calculated at temperature T_h. Obviously, once the Nusselt numbers for the cooled half cylinder are known from eqs. (28) and (29), the corresponding Nusselt numbers for the heated half cylinder can be evaluated through eq. (26). Finally, it can be noticed that the optimal particle loading for maximum heat transfer, φ_{opt}, depends substantially on the average temperature and the imposed temperature difference, while it is almost independent of the other controlling parameters, which gives the opportunity to develop the following easy-to-apply

Figure 9. Comparison between the predictions of eqs. (28) and (29) and the numerical data of Nu_{fc} and Nu_c

dimensional correlation useful to evaluate φ_{opt} as a function of t_{av} (expressed in degrees centigrade) and ΔT:

$$\varphi_{opt} = (9 \cdot 10^{-5})\left[t_{av}(°C)\right]^{1.5} \Delta T^{0.13} \tag{32}$$

with a 2.9% standard deviation of error and a 5% range of relative error.

Conclusions

Laminar natural convection of nanofluids in differentially-heated horizontal semi-annuli has been studied numerically by the way of a two-phase model based on the double-diffusive approach, in the hypothesis that Brownian diffusion and thermophoresis are the only slip mechanisms by which the solid phase can develop a significant relative velocity with respect to the liquid phase. The four-equation system of the mass, momentum, and energy transfer governing equations has been solved using a computational code relying on the SIMPLE-C algorithm which incorporates three empirical correlations for the evaluation of the effective thermal conductivity, the effective dynamic viscosity, and the thermophoretic diffusion coefficient, all based on a high number of experimental data available in the literature.

Simulations have been performed for water-based nanofluids with suspended Al_2O_3 or CuO or TiO_2 nanoparticles, for different values of the average volume fraction of the suspended solid phase in the range 0-0.04, the diameter of the nanoparticles in the range 25-75 nm, the average temperature in the range 300-330 K, the temperature difference imposed across the cavity in the range 5-20 K, the diameter of the inner half cylinder in the range 0.03-0.07 m, and the ratio between the diameters of the outer and inner half cylinders in the range 2-4.

The main results obtained may be summarized as follows.

- The overall solid phase migration from hot to cold results in a co-operating solutal buoyancy force which tends to compensate the friction increase consequent to the viscosity growth due to the dispersion of the nanoparticles into the base fluid.
- The effect of the increased thermal conductivity consequent to the nanoparticle dispersion into the base fluid plays the major role in determining the heat transfer enhancement of the nanofluid, at least in the upper range of the investigated average temperatures.

- At high and intermediate temperatures, the nanofluid heat transfer performance relative to that of the pure base liquid increases with increasing the average volume fraction of the suspended nanoparticles, whereas at low temperatures has a peak at an optimal particle loading.
- The relative heat transfer performance of the nanofluid increases notably with increasing the average temperature, moderately as the diameter of the inner half cylinder and the imposed temperature difference are decreased, and faintly as the diameter ratio is increased.
- At low temperature, the relative heat transfer performance of the nanofluid increases slightly as the nanoparticle size decreases at low solid-phase volume fractions, whereas it decreases at high volume fractions.
- At high temperature, the relative heat transfer performance of the nanofluid increases as the nanoparticle size decreases.
- At temperatures of the order of the room temperature, the relative heat transfer performance of the nanofluid is notably higher for $Al_2O_3 + H_2O$ than for $CuO + H_2O$ and even more than for $TiO_2 + H_2O$, whereas the solid phase effect is much less remarkable as temperature is increased.

Nomenclature

c – specific heat at constant pressure, [$Jkg^{-1}K^{-1}$]
D_B – Brownian diffusion coefficient, [m^2s^{-1}]
D_i – diameter of the inner cylinder, [m]
D_T – thermophoretic diffusion coefficient, [m^2s^{-1}]
d_f – equivalent diameter of a base fluid molecule, [m]
d_p – nanoparticle diameter, [m]
$\vec{g}$ – gravity vector, [ms^{-2}]
h – average coefficient of convection, [$Wm^{-2}K^{-1}$]
$\mathbf{I}$ – unit tensor, [–]
$\vec{J}_p$ – nanoparticle diffusion mass flux, [$kgm^{-2}s^{-1}$]
k – thermal conductivity, [$Wm^{-1}K^{-1}$]
k_b – Boltzmann constant (= $1.38066 \cdot 10^{-23}$), [JK^{-1}]
M – molecular weight of the base fluid, [$gmol^{-1}$]
m – nanoparticle mass fraction, [–]
N – Avogadro number (= $6.022 \cdot 10^{23}$), [mol^{-1}]
Nu – Nusselt number (= hD/k), [–]
Pr – Prandtl number (= $\mu c/k$), [–]
p – pressure, [Pa]
Q – heat transfer rate, [W]
q – heat flux, [Wm^{-2}]
R_i – radius of the inner cylinder, [m]
R_o – radius of the outer cylinder, [m]
Ra – Rayleigh number (= $\rho cg|\Delta\rho|D_i^3/\mu k$), [–]
Re_p – nanoparticle Reynolds number, [–]
r – radial co-ordinate, [m]
S_T – thermophoresis parameter, [–]
T – temperature, [K]

t – time, [s]
t_D – time required for a nanoparticle to move by a distance equal to its diameter, [s]
U – radial velocity component, [ms^{-1}]
u_p – nanoparticle Brownian velocity, [ms^{-1}]
V – tangential velocity component, [ms^{-1}]
$\bar{V}$ – velocity vector, [ms^{-1}]
V_m – molecular volume

Greek symbols

δ – diameter ratio, [–]
θ – angular co-ordinate, [°]
φ – nanoparticle volume fraction, [–]
μ – dynamic viscosity, [$kgm^{-1}s^{-1}$]
ρ – mass density, [kgm^{-3}]
$\boldsymbol{\tau}$ – stress tensor, [$kgm^{-1}s^{-2}$]

Subscripts

av – average
c – cooled half cylinder, at the temperature of the cooled half cylinder
f – base fluid
fr – freezing point of the base fluid
h – heated half cylinder, at the temperature of the heated half cylinder
max – maximum value
min – minimum value
n – nanofluid
s – solid phase

References

[1] Abu-Nada, E., *et al.*, Natural Convection Heat Transfer Enhancement in Horizontal Concentric Annuli Using Nanofluids, *Int. Comm. Heat Mass Transfer, 35* (2008), 5, pp. 657-665
[2] Abu-Nada, E., Effects of Variable Viscosity and Thermal Conductivity of Al_2O_3-Water Nanofluid on Heat Transfer Enhancement in Natural Convection, *Int. J. Heat Fluid Flow, 30* (2009), 4, pp. 679-690

Quintino, A., *et al.*: Buoyancy-Induced Convection of Water-Based Nanofluids in ...
THERMAL SCIENCE: Year 2017, Vol. 21, No. 6A, pp. 2643-2660

2659

[3]   Abu-Nada, E., Effects of Variable Viscosity and Thermal Conductivity of CuO-Water Nanofluid on Heat Transfer Enhancement in Natural Convection: Mathematical Model and Simulation, *J. Heat Transfer, 132* (2010), 5, 052401

[4]   Soleimani, S., *et al.*, Natural Convection Heat Transfer in a Nanofluid Filled Semi-Annulus Enclosure, *Int. Comm. Heat Mass Transfer, 39* (2012), 4, pp. 565-574

[5]   Yu, Z.-T., *et al.*, A Numerical Investigation of Transient Natural Convection Heat Transfer of Aqueous Nanofluids in a Horizontal Concentric Annulus, *Int. J. Heat Mass Transfer, 55* (2012), 4, pp. 1141-1148

[6]   Parvin, S., *et al.*, Thermal Conductivity Variation on Natural Convection Flow of Water-Alumina Nanofluid in an Annulus, *Int. J. Heat Mass Transfer, 55* (2012), 19-20, pp. 5268-5274

[7]   Ashorynejad, H. R., *et al.*, Magnetic Field Effects on Natural Convection Flow of a Nanofluid in a Horizontal Cylindrical Annulus Using Lattice Boltzmann Method, *Int. J. Thermal Sciences, 64* (2013), Feb., pp. 240-250

[8]   Sheikholeslami, M., *et al.*, Effect of a Magnetic Field on Natural Convection in an Inclined Half-Annulus Enclosure Filled with Cu-Water Nanofluid Using CVFEM, *Advanced Power Technology, 24* (2013), 6, pp. 980-991

[9]   Corcione, M., *et al.*, A Two-Phase Numerical Study of Buoyancy-Driven Convection of Alumina-Water Nanofluids in Differentially-Heated Horizontal Annuli, *Int. J. Heat Mass Transfer, 65* (2013), Oct., pp. 327-338

[10] Sheikhzadeh, G. A., *et al.*, Laminar Natural Convection of Cu-Water Nanofluid in Concentric Annuli with Radial Fins Attached to the Inner Cylinder, *Heat Mass Transfer, 49* (2013), 3, pp. 391-403

[11] Sheikholeslami, M., Ganji, D. D., Ferrohydrodynamic and Magnetohydrodynamic Effects on Ferrofluid Flow and Convective Heat Transfer, *Energy, 75* (2014), Oct., pp. 400-410

[12] Sheikholeslami, M., *et al.*, Thermal Management for Free Convection of Nanofluid Using Two Phase Model, *J. Mol. Liq.*, *194* (2014), June, pp. 179-187

[13] Arbaban, M., Salimpour, M. R., Enhancement of Laminar Natural Convective Heat Transfer in Concentric Annuli with Radial Fins Using Nanofluids, *Heat Mass Transfer, 51* (2015), 3, pp. 353-362

[14] Fallah, K., *et al.*, Simulation of Natural Convection Heat Transfer Using Nanofluid in a Concentric Annulus, *Thermal Science*, 21 (2017), 3, pp. 1275-1286

[15] Bezi, S., *et al.*, Enhancement of Natural Convection Heat Transfer Using Different Nanoparticles in an Inclined Semi-Annular Enclosure Partially Heated From above, *High Temp., 53* (2015), 1, pp. 99-117

[16] Seyyedi, S. M., *et al.*, Natural Convection Heat Transfer under Costant Heat Flux Wall in a Nanofluid Filled Annulus Enclosure, *Ain Shams Eng. J., 6* (2015), 1, pp. 267-280

[17] Oglakkaya, F. S., Bozkaya, C., MHD Natural Convection in a Semi-Annulus Enclosure Filled with Water-Based Nanofluid Using DRBEM, *Eng. Anal. Bound. Elem., 71* (2016), Oct., pp. 151-163

[18] Zhang, C., *et al.*, Unsteady Natural Convection Heat Transfer of Nanofluid in an Annulus with Sinusoidally Heated Source, *Num. Heat Transfer, 69* (2016), 1, pp. 97-108

[19] Sheikholeslami, M., Chamka, A. J., Electrohydrodynamic Free Convection Heat Transfer of a Nanofluid in a Semi-Annulus Enclosure with a Sinusoidal Wall, *Num. Heat Transfer, 69* (2016), 7, pp. 781-793

[20] Maxwell, J. C., *A Treatise on Electricity and Magnetism*, 3rd ed., Mineola, Dover, N. Y., USA, 1954

[21] Brinkman, H. C., The Viscosity of Concentrated Suspensions and Solutions, *J. Chem. Phys.*, *20* (1952), 4, p. 571

[22] McNab, G. S., *et al.*, Thermophoresis in Liquids, *J. Colloid Interface Science, 44* (1973), 2, pp. 339-346

[23] Buongiorno, J., Convective Transport in Nanofluids, *J. Heat Transfer, 128* (2006), 3, pp. 240-250

[24] Das, S. K., *et al.*, Pool Boiling Characteristics of Nano-Fluids, *Int. J. Heat Mass Transfer, 46* (2003), 5, pp. 851-862

[25] Prasher, R., *et al.*, Measurements of Nanofluid Viscosity and its Implications for Thermal Applications, *Appl. Phys. Lett.*, *89* (2006), 13, 133108

[26] He, Y., *et al.*, Heat Transfer and Flow Behaviour of Aqueous Suspensions of TiO_2 Nanoparticles (Nanofluids) Flowing Upward through a Vertical Pipe, *Int. J. Heat Mass Transfer, 50* (2007), 11-12, pp. 2272-2281

[27] Chen, H., *et al.*, Rheological Behaviour of Ethylene Glycol Based Titania Nanofluids, *Chem. Phys. Lett.*, *444* (2007), 4-6, pp. 333-337

[28] Chevalier, J. *et al.*, Rheological Properties of Nanofluids Flowing through Microchannels, *Appl. Phys. Lett., 91* (2007), 23, pp. 233103

[29] Cabaleiro, D., *et al.*, Characterization and Measurements of Thermal Conductivity, Density and Rheological Properties of Zinc Oxide Nanoparticles Dispersed in (Ethane-1,2-diol + Water) Mixture, *J. Chem. Thermodynamics, 58* (2013), Mar., pp. 405-415

2660

Quintino, A., *et al.*: Buoyancy-Induced Convection of Water-Based Nanofluids in ...
THERMAL SCIENCE: Year 2017, Vol. 21, No. 6A, pp. 2643-2660

[30] Einstein, A., Uber die von der molekularkinetischen Theorie der Warme geforderte Bewegung von in ruhenden Fluessigkeiten suspendierten Teilchen (in German), *Ann. Phys.*, *322* (1905), 8, pp. 549-560

[31] Corcione, M., *et al.*, Enhanced Natural Convection Heat Transfer of Nanofluids in Enclosures with Two Adjacent Walls Heated and the Two Opposite Walls Cooled, *Int. J. Heat Mass Transfer,* 88 (2015), Sept., pp. 902-913

[32] Corcione, M., Empirical Correlating Equations for Predicting the Effective Thermal Conductivity and Dynamic Viscosity of Nanofluids, *Energy Convers. Management, 52* (2011), 1, pp. 789-793

[33] Keblinski, P., *et al.*, Mechanisms of Heat Flow in Suspensions of Nano-Sized Particles (Nanofluids), *Int. J. Heat Mass Transfer, 45* (2002), 4, pp. 855-863

[34] Corcione, M., *et al.*, Two-Phase Mixture Modeling of Natural Convection of Nanofluids with Temperature-Dependent Properties, *Int. J. Thermal Sciences, 71* (2013), Sept., pp. 182-195

[35] Ghanbarpour, M., *et al.*, Thermal Properties and Rheological Behavior of Water Based Al_2O_3 Nanofluid as a Heat Transfer Fluid, *Exp. Thermal Fluid Science, 53* (2014), Feb., pp. 227-235

[36] Akilu, S., *et al.*, A Review of Thermophysical Properties of Water Based Composite Nanofluids, *Renew. Sustain. Energy Rev., 66* (2016), Dec., pp. 654-678

[37] Pak, B. C., Cho, Y., Hydrodynamic and Heat Transfer Study of Dispersed Fluids with Submicron Metallic Oxide Particles, *Exp. Heat Transfer, 11* (1998), 2, pp. 151-170

[38] Zhou, S. Q., Ni, R., Measurement of the Specific Heat Capacity of Water-Based Al_2O_3 Nanofluid, *Appl. Phys. Lett., 92* (2008), 9, 093123

[39] Van Doormaal, J. P., Raithby, G. D., Enhancements of the Simple Method for Predicting Incompressible Fluid Flows*, Num. Heat Transfer, 7* (1984), 2, pp. 147-163

[40] Patankar, S. V., Spalding, D. B., A Calculation Procedure for Heat, Mass and Momentum Transfer in Three-Dimensional Parabolic Flows, *Int. J. Heat Mass Transfer, 15* (1972), 10, pp. 1787-1797

[41] Patankar, S. V., *Numerical Heat Transfer and Fluid Flow*, Hemisphere Publ. Co., Washington, DC, 1980

[42] Leonard, B. P., A Stable and Accurate Convective Modelling Procedure Based on Quadratic Upstream Interpolation, *Comp. Meth. Appl. Mech. Eng., 19* (1979), 1, pp. 59-78

[43] Kuehn, T. H., Goldstein, R. J., An Experimental and Theoretical Study of Natural Convection in the Annulus Between Horizontal Concentric Cylinders, *J. Fluid Mech.*, *74* (1976), 4, pp. 695-719

[44] Phanikumar, M. S., Mahajan, R. L., Numerical Analysis of Unsteady Thermosolutal Convection over a Horizontal Isothermal Circular Cylinder, *Num. Heat Transfer, 33* (1998), 7, pp. 673-700

[45] Putra, N., *et al.*, Natural Convection of Nano-Fluids, *Heat Mass Transfer, 39* (2003), 8-9, pp. 775-784

[46] Chang, B. H., *et al.*, Natural Convection of Microparticle Suspensions in Thin Enclosures, *Int. J. Heat Mass Transfer, 51* (2008), 5-6, pp. 1332-1341

[47] Hu, Y., *et al.*, Experimental and Numerical Study of Natural Convection in a Square Enclosure Filled with Nanofluid, *Int. J. Heat Mass Transfer, 78* (2014), Nov., pp. 380-392

[48] Wen, D. Ding, Y., Formulation of Nanofluids for Natural Convective Heat Transfer Applications, *Int. J. Heat Fluid Flow, 26* (2005), 6, pp. 855-864